ELECTRONIC STRUCTURE AND STABILIZATION OF C60 FULLERENES ENCAPSULATING ACTINIDE ATOM

M. V. Ryzhkov[1,*], A. L. Ivanovskii[1], B. Delley[2]

[1]Institute of Solid State Chemistry, Ural Branch of the Russian Academy of Sciences, 620990, Ekaterinburg, Russia

[2]Paul Scherrer Institut WHGA 123, CH-5232, Villigen PSI, Switzerland

*ryz@ihim.uran.ru

PACS 31.15A, 31.15ae, 31.15aj, 31.15E

The geometry optimization of the neutral molecules An@C_{60} (An = Th – Md) was carried out using the DFT based Dmol^3 method. In order to perform calculations for these complexes' electronic structures, the fully relativistic discrete variational method (RDV) was used. Two types of stable position of metal atom inside the C_{60} cage were obtained. The most stable non-central positions are favored over the position of actinide in the fullerene center for all An@C_{60} complexes. Systems containing light actinides have considerable energetic stability, which is noticeably greater than that of corresponding exohedral and "networked" complexes. The 5f-orbitals' contribution to chemical bonding was found to be noticeably less than that of the 6d-states, even for the complexes at the beginning of An@C_{60} row. The effective charges on the actinide atoms were calculated using integral scheme incorporated in RDV and Hirshfeld procedure of DMol^3 code.

Keywords: fullerenes, actinides, ab initio methods, relativistic calculations, molecular structure, stability.

1.   Introduction

The earlier investigations of charged and neutral endohedral fullerenes An@C_{28} (An = Th – Md) [1,2] as well as An@C_{40} (An = Th – Md) [3] showed that some of these clusters can be very stable and therefore, may be useful for nuclear applications such as medicine or nuclear waste disposal. Since the discovery of C_{60} [4], these fullerenes have been widely studied both experimentally and theoretically. To date, we know only one actinide endohedral system U@C_{60}, which has been obtained experimentally, Diener et al. [5] reported that U@C_{60} was produced by subliming fullerenes from arc-produced soot onto a mass spectrometry target. Chang et al. [6] theoretically predicted its properties, according to these Restricted Hartree-Fock calculations the U@C_{60} and U$^+$@C_{60} complexes should be less stable than separated C_{60} and U. However, in Ref. [6] only one central position of various atoms inside the icosahedral carbon cage was considered. On the other hand, the radius of this fullerene (nearly 3.6 Å) is evidently too large for one actinide atom or ion, so the An@C_{60} structure with metal site just in the center of the cage could be less favorable than those where actinide atom is shifted to the cage wall and interacts with only few carbon neighbors.

Interest in C_{60} fullerene-encapsulated actinide atoms is also due to the possibility of 5f – states participation in bonding. It is evident that theoretical study of the electronic structure and chemical bonding of any systems containing actinides requires the inclusion of all relativistic effects in the computational method. The fully relativistic calculations of An@C_{28} clusters (An = Th – Md) [2] showed that 5f orbitals participate in chemical

bonding of the first half of this series from $Th@C_{28}$ to $Cm@C_{28}$. Conversely, in the fully relativistic calculations of $An@C_{40}$ complexes (An = Th – Md) [3], we determined that An5f contributions to bonding are nearly three times less than that of the main An6d–C2p interaction even in the clusters at the beginning of this row ($Th@C_{40}$ and $Pa@C_{40}$). These results are in agreement with the known sensitivity of 5f bonding features to the variation of bond-lengths, because an average radius of fullerene cage increases from 2.5 Å (C_{28}) to 3 Å (C_{40}). Since the radius of C_{60} molecule is close to 3.6 Å, one can expect that in a case of central position of metal atom the role of 5f states in bonding will be noticeably less than in $An@C_{40}$. On the other hand, some shift of actinide atom from the center to the cage wall can reduce the An–C bond lengths to the values, which are more typical for the An–C interactions in the molecules and solids.

The aim of the present paper was the search for most stable positions of actinide atom inside a C_{60} cage, the evaluation of geometrical parameters of the neutral $An@C_{60}$ complexes for almost all actinides from Th to Md, the investigations of the chemical bonding and the role played by 5f states in the interaction between metal atom and the carbon shell. Another aim of the work presented here was the comparison of binding energies of the three competitive types of structures: (1) endohedral $An@C_{60}$; (2) exohedral AnC_{60}, where the actinide atom is bound to C_{60} from the outside of the cage; (3) "networked" $C_{59}An$, where the actinide atom is incorporated into the C_{60} cage, at least in the cases of most stable complexes. The results of present calculations also allow us to evaluate the electron density redistribution for various positions of metal atom and across this series.

2. Objects and methods of calculations

Geometry optimization of "empty" C_{60} molecule with I_h symmetry and C_{60} interacting with actinide atoms was performed using the DMol^3 method [7] in the scalar relativistic approach [8] and with the largest double numerical atomic basis set ("dnp"). The Coulombic potential was computed with the use of model density obtained as decomposition of charge density into multipolar components including those with l = 3. The generalized gradient approximation (GGA) in "BLYP" [10,11] and "PBE" [9] forms was used in all calculations. In a previous paper [2], we used "PBE" as well as "BLYP" [10,11] functionals, as was shown, the energetic and geometrical parameters obtained using both approaches were similar. Optimization of the molecular structures was done until the change in the maximum energy gradient values was less than 0.001 atomic unit, the global orbital cutoff was 8.0 Å. To confirm that the stationary points correspond to minima, the vibrational frequencies were computed for all clusters. To test the reliability of parameters used in the calculations, we performed geometry optimization for $Th@C_{60}$, $Am@C_{60}$ and $Md@C_{60}$ systems using the multipolar components with l = 4 and 10 Å for orbital cutoff. Though the computer time increased considerably, the changes in energy were less than 0.05 eV and the shifts in atomic coordinates were less than 10^{-3} Å.

For the investigation of the nature of chemical bonding and the role played by 5f electrons in $An@C_{60}$ complexes, we also used the fully relativistic discrete variational method (RDV) [12,13]. For the most stable geometrical structures obtained by DMol^3, RDV calculations were performed. The RDV method is based on the solution of the Dirac-Slater equation for four-component wave functions, transforming according to irreducible representations of the double point group (C_S^* and C_{2V}^* in the present calculations). For calculation of the symmetry coefficients, we used the original code which realizes the projection-operators technique [12] and includes the matrices of irreducible representations of double point groups obtained in Ref. [14] and the transformation matrices presented in Ref. [15]. The extended

bases of four-component numerical atomic orbitals (AO) obtained as the solution of the Dirac-Slater equation for isolated neutral atoms also included $An7p_{1/2}$ and $7p_{3/2}$ functions in addition to occupied AOs. Numerical Diophantine integration in matrix elements calculations was done for 126000 sample points, which provided the convergence of valence MO energies within 0.1 eV. The effective charges on atoms (Q_{eff}) were computed as integrals of electron density inside the domains bounded by the points of its minimum [16].

3. Results and Discussion

3.1. Results of geometry optimization

It is well known that optimized structure of $C_{60}(I_h)$ consists of 12 regular pentagons and 20 hexagons (Fig. 1). In our DMol calculations, we obtained that the radius for the empty fullerene is close to 3.55 Å. This value for the cage radius corresponds to the C–C bond lengths in pentagons and hexagons in the range 1.46 – 1.40 Å. In the calculations of Chang et al. [6] the interval of C–C bond lengths in $C_{60}(I_h)$ was slightly wider: 1.45 – 1.37 Å. For the evaluation of the relative stability of various $An@C_{60}$ complexes, it is reasonable to consider the binding energy E_b (which is sometimes called the "total bond energy" or the "atomization energy"). The binding energy of a cluster is usually defined as $E_b = E_{tot} - E_{sum}$, where E_{tot} is the total energy of a cluster and E_{sum} is the sum of total energies of all isolated atoms in the cluster. The binding energies for all investigated fullerenes are summarized in Table 1.
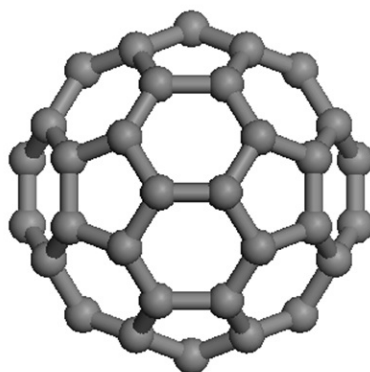

FIG. 1. The geometrical structure of fullerene C_{60}

We started by modeling the most symmetrical central position of actinide atom inside the C_{60} cage, the values of $E_b(I_h)$ obtained in these calculations are shown in the second column of Table 1. Comparison of the E_b values for C_{60} and $An@C_{60}$ allows one to evaluate the stability of $An@C_{60}$ clusters with respect to the dissociation limit $An + C_{60}$ for all actinides. According to our results, the symmetrical complexes of Pa, U and Np are stable systems and the most stable one is $Np@C_{60}$ with $Np + C_{60}$ dissociation energy near 3.1 eV. In the cases of smaller endohedral fullerenes $An@C_{28}$ [2] and $An@C_{40}$ [3], the $Pa@C_n$ were the most stable complexes with corresponding dissociation energies near 8.1 and 6.4 eV respectively. Although the stability of $An@C_{60}$ (I_h) obtained in the present calculations is considerably less than that of the corresponding $An@C_{28}$ and $An@C_{40}$, the uranium encapsulation reaction $U + C_{60} \rightarrow U@C_{60}$ (Table 1) is still exothermic (2.6 eV), whereas according to the results of Chang et al. [6] the $U@C_{60}$ complex should be noticeably less stable than separated C_{60} and U (by ~ 3.5 eV). The analysis of geometrical parameters obtained for $An@C_{60}$ (I_h) shows

TABLE 1. Binding and dissociation energies (eV), distances (Å) between the actinide atom and the nearest C atoms and effective charges (e) on actinide atoms in the investigated complexes

Complex	E_b (I_h)	E_b (C_s, C_{2v})	E_d (C_s, C_{2v})	R_{An-C} (C_s, C_{2v})	Q_{An} (C_s, C_{2v})	
					Hirshfeld	Integral
C_{60}	-452.7	-	-	-	-	
Th@C_{60}	-454.3	-458.5(C_s)	5.8	2.50 / 2.50 / 2.50	0.68	2.17
Pa@C_{60}	-455.0	-459.3(C_s)	6.6	2.44 / 2.44 / 2.44	0.71	1.93
U@C_{60}	-455.3	-458.9(C_s)	6.2	2.41 / 2.43 / 2.44	0.63	1.83
Np@C_{60}	-455.8	-458.4(C_s)	5.7	2.42 / 2.43 / 2.44	0.57	1.74
Pu@C_{60}	-453.5	-455.2(C_{2v})	2.5	2.36 / 2.51 / 2.51	0.66	1.41
Am@C_{60}	-453.3	-454.3(C_{2v})	1.6	2.36 / 2.52 / 2.52	0.62	1.34
Cm@C_{60}	-453.4	-454.5(C_{2v})	1.8	2.46 / 2.61 / 2.61	0.60	1.35
Bk@C_{60}	-453.4	-454.4(C_s)	1.7	2.60 / 2.61 / 2.63	0.75	1.22
Cf@C_{60}	-453.4	-454.4(C_s)	1.7	2.64 / 2.65 / 2.66	0.73	1.23
Es@C_{60}	-453.4	-454.2(C_s)	1.5	2.65 / 2.67 / 2.69	0.72	1.15
Fm@C_{60}	-453.4	-453.6(C_s)	0.9	2.65 / 2.67 / 2.70	0.62	1.14
Md@C_{60}	-453.4	-453.5(C_s)	0.8	2.78 / 2.79 / 2.79	0.64	1.06
PaC_{60}	-	-455.7	3.0	2.34	0.58	1.73
C_{59}Pa	-	-448.8	-3.9	2.17 / 2.25 / 2.25	0.78	2.44

that the deformation of the cage due to addition of any actinide atom is small: the radial expansion of the cage is less than 0.01 Å in all clusters.

The search for less symmetrical An@C_{60} structures was undertaken in a few ways: the various shifts of metal atom from the center in different directions were considered. These initial configurations were subjected to geometry optimization, leading to new stable, but less symmetrical An@C_{60} structures. The values of initial shift of actinide atom varied from 0.1 to 0.6 Å. However, small shifts (0.1 – 0.3 Å) led to a relaxation of the system into structures with An atom located near the center of C_{60} shell. Conversely, a shift of metal atom by 0.4 Å or greater led to rearrangement of the complex into a structure with an actinide atom located near the cage wall. This result means that the potential barrier for transformation of the geometry with central actinide position is quite small. The optimized structures with various symmetries were obtained (C_{2v}, C_s, C_1). According to results of DMol calculations, we can predict that there are two types of most stable geometry for "distorted" endohedral fullerenes, corresponding to C_s and C_{2v} symmetries. The structures of these complexes are illustrated in Figure 2. Though the difference in binding energy for these two isomers for each An@C_{60} cluster is within 0.1 eV, we can conclude that for complexes of Th, Pa, U and Np, the former type (C_s) is slightly more stable and should be considered as the ground structure. For the three clusters in the middle of the row (Pu, Am, Cm) the C_{2v} – isomer appeared to be slightly more stable. For the "end part" of the row from Bk to Md the E_b for C_s structures is slightly lower than that for C_{2v} isomers. The binding and dissociation energy values obtained for these structures are shown in the third and the fourth columns of Table 1 respectively. As can be seen from Fig. 2, in both "distorted" isomers, the actinide

atom has six nearest carbon neighbors, which belong to one hexagon in C_s – structure and to the two adjacent hexagons ("X" – shape of carbon vicinity) in the C_{2v} structure.
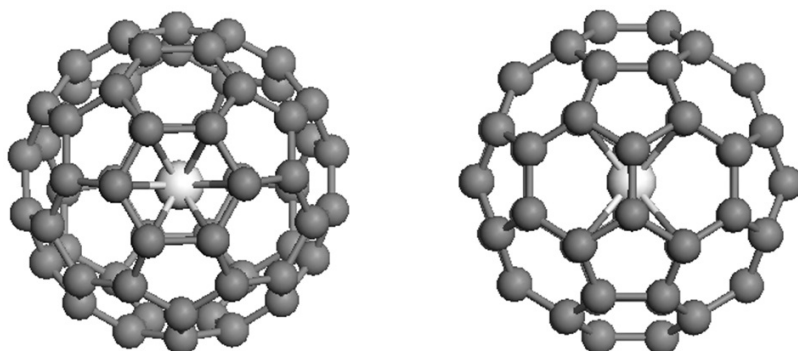

FIG. 2. The geometrical structures of endohedral complexes $An@C_{60}$ corresponding to C_s (left) and C_{2v} (right) symmetry

According to our results, complexes of Th, Pa, U and Np are more stable systems with An + C_{60} dissociation energy near 6 eV. The most stable cluster is $Pa@C_{60}$ with a dissociation energy close to 6.6 eV. As mentioned above, in the cases of smaller endohedral fullerenes the most stable complexes were also formed by encapsulation of protactinium atom [2,3]. It is interesting that stable systems were also obtained in the second half of the $An@C_{60}$ row: the complexes of Cm, Bk Cf and Es are noticeably more stable than separated C_{60} and An. Note that stable clusters for heavier actinides were also predicted for $An@C_{40}$ systems [3], moreover, for $An@C_{60}$ clusters the similar non-monotonic trend is obtained, particularly, in the case of $Am@C_{60}$ the absolute value of E_b is less than that for $Cm@C_{60}$. As can be seen, the values of E_b for all isomers of $Fm@C_{60}$ and $Md@C_{60}$ (near –453.5 eV) are lower than that of empty C_{60} (–452.7 eV).

The values of An–C bond lengths for the nearest carbon neighbors in the C_s and C_{2v} structures are shown in the fifth column of Table 1. Though the shapes of hexagons and pentagons in C_s and C_{2v} structures are very close to regular geometry of an empty C_{60}, the six nearest neighbors of actinide atom belong to the three and two nonequivalent types in C_s and C_{2v} isomers respectively. These atoms are labeled later as C1, C2 and C3 (C_s), while in C_{2v} clusters the two pairs of carbon atoms of C2 and C3 types are equivalent. In each complex of the C_s – type containing Th, Pa, U, Np and from Bk to Md, the distances between metal atom and C1, C2 and C3 are close to each other (Table 1). These results mean that the actinide atom is located just under the center of one hexagon. For the molecules of C_{2v} type ($Pu@C_{60}$, $Am@C_{60}$, $Cm@C_{60}$) we obtained noticeable variation of these bond lengths (by 0.15 – 0.16 Å). As can be seen, there is no complete correlation between the variation of average values of An–C bond lengths in $An@C_{60}$ row and the main trend of E_b variation, however, the increase of stability from $Th@C_{60}$ to $Pa@C_{60}$ and its decrease from $Pa@C_{60}$ to $Am@C_{60}$ and from $Cm@C_{60}$ to $Md@C_{60}$ are accompanied by the decrease and increase of corresponding An–C distances, as could be expected from general consideration. There is one noticeable exception to this rule: the An–C bond lengths in the less stable $Am@C_{60}$ are less than those in the more stable $Cm@C_{60}$, $Bk@C_{60}$ and $Cf@C_{60}$ complexes.

In Table 1 we also show the results obtained for the most stable example of exohedral fullerene (PaC_{60}) and "networked" complex ($C_{59}Pa$). The exohedral structures were generated from empty C_{60} particle by the addition of Pa atom from several spatial directions. These initial configurations were subjected to geometry optimization, leading to a few stable

structures. The lowest-energy C$_{2v}$ isomer is a distorted C$_{60}$ fullerene, with the metal atom bonded to a pair of carbon atoms, another isomer, in which the actinide atom interacts with carbon hexagon appeared to be slightly less stable. The structure of this complex is illustrated in Figure 3. We obtained that in these complexes Pa–C distances are near 2.34 Å. The absolute value of binding energy of this most stable exohedral complex was found to be 455.7 eV, this value is noticeably less than that for the non-central endohedral position of Pa inside C$_{60}$ cage (459.3 eV). However, the value of $|E_b|$ for exohedral cluster was greater than that for endohedral position in the center of fullerene (455.0 eV). Thus, the dissociation energy of PaC$_{60}$ complex with respect to the PaC$_{60}$ →Pa + C$_{60}$ reaction is more than two times less than that obtained for the non-central endohedral position of protactinium atom. The distortion of fullerene cage in the PaC$_{60}$ (C$_{2v}$) molecule due to interaction with metal atom led to increase of the number of non-equivalent carbon sites. However, the average value of r(C) in PaC$_{60}$ system is close to the corresponding parameter of endohedral complex.

The "networked" C$_{59}$Pa structure was generated from an empty C$_{60}$ particle by the substitution of an actinide atom for a carbon site. Then, this initial structure was subjected to geometry optimization, leading to the new equilibrium positions for the metal and carbon atoms (Fig. 3). The parameters of this cluster were shown in Table 1. In contrast to endohedral and exohedral systems, the "networked" complex is less stable than an empty C$_{60}$ cage (Table 1). This result is quite expected because the C–C bonds are certainly stronger than C–An bonds in such systems. We also obtained that during geometry optimization of C$_{59}$An structure the initial distances between metal atom and the cage center increased from 3.55 Å to 4.96 Å. This considerable increase in the distances between metal atom and the center of the cage is accompanied by a corresponding increase in the bond lengths between actinide atom and its three nearest neighbors: these distances were found to be 2.17 Å, 2.25 Å and 2.25 Å. Nevertheless, the interatomic Pa–C distances in C$_{59}$Pa as well as in PaC$_{60}$ are noticeably less than those in more stable endohedral complex (2.44 Å).
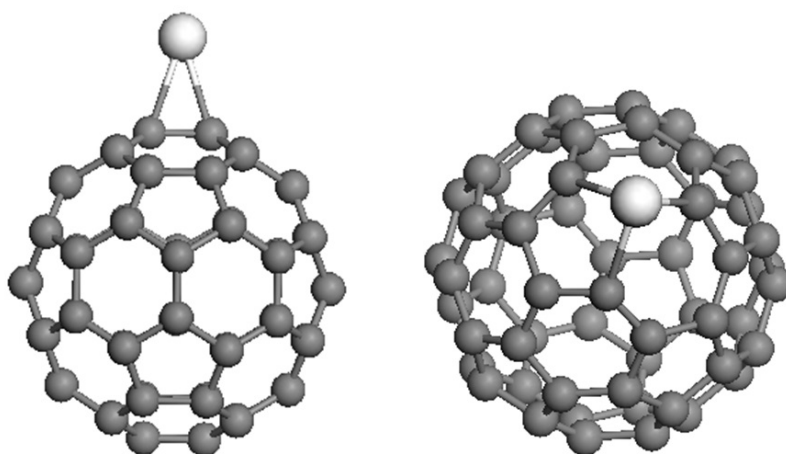

FIG. 3. The geometrical structures of exohedral PaC$_{60}$ (left) and "networked" C$_{59}$Pa (right) complexes

As mentioned above, the present DMol results were obtained in the scalar relativistic approach, however, the authors [1] evaluated the role of spin-orbit coupling in the Pu^{4+}@C$_{28}$ cluster and showed that the addition of these effects caused a maximum expansion of the Pu–C distance of 0.027 Å with respect to the scalar relativistic results. They also reported

that the scalar relativistic bonding energy of the $Pu^{4+}@C_{28}$ increased by less than 8% when the spin-orbit coupling effects were included in the calculations.

3.2. RDV calculations

In Figure 4 we show the partial densities of states (DOS) obtained in the fully relativistic RDV calculations for the ground state isomers of $Th@C_{60}$ and $Pa@C_{60}$ clusters. In the cases of C2s and C2p DOS we show only the contributions from C1, C2 and C3 atoms, which are the nearest neighbors of metal ion. As can be seen from Fig. 4, the spin-orbital interaction is small for the "outer" bands, particularly the 0.9 eV splitting was obtained for $An5f_{5/2}$ and $An5f_{7/2}$ main peaks. The relativistic effects become considerable for deeper orbitals, that is, the main peak of $An6p_{1/2}$ band is shifted to the lower energies by ~ 9 eV (Th) and ~ 10 eV (Pa) from the highest intensity peak of $An6p_{3/2}$ DOS. In both complexes the most intensive part of occupied valence C2p band in the energy region from 0 to –10 eV (Fermi level is used as a zero of energy scale) contains some contributions from An6d AOs (near -6 – -4 eV) and An5f AOs (near -5 – 0 eV). The vacant MOs are formed by C2p, An5f, 6d, 7s and 7p orbitals in the energy region from 0 to 19 eV.
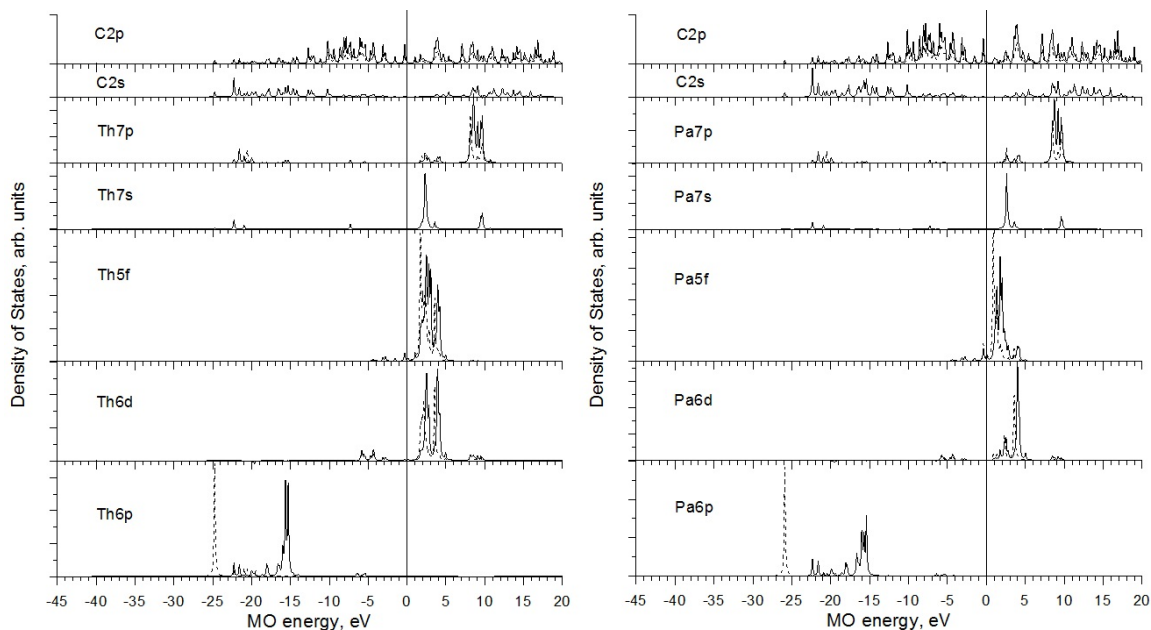

FIG. 4. Partial densities of states for the ground isomers of $Th@C_{60}$ (left) and $Pa@C_{60}$ (right) clusters. The broken lines correspond to $p_{1/2}$, $d_{3/2}$, and $f_{5/2}$ DOS, the solid lines correspond to $p_{3/2}$, $d_{5/2}$ and $f_{7/2}$ DOS (vertical line is the border between occupied and vacant states)

The energy gap between occupied and vacant molecular states, defined as the difference of energy of the highest occupied (HOMO) and the lowest unoccupied (LUMO) molecular orbitals, obtained in our relativistic calculations for $Th@C_{60}$, is near 0.4 eV. In similar calculations for $Th@C_{28}$ [2] and $Th@C_{40}$ [3], we obtained considerably greater HOMO – LUMO gaps (2.3 and 1.4 eV respectively). The latter gap values were noticeably greater than those for the empty C_{40} and C_{28} cages (near 0.05 and 0.6 eV respectively), on the other hand, the energy gap in empty C_{60} cage (1.6 eV) is considerably greater than that in any $An@C_{60}$ cluster studied in the present work. In $Th@C_{60}$ and $Pa@C_{60}$ complexes both the HOMO and LUMO are of predominantly C2p character with small contributions from

An5f states. According to our results, the Fermi level in Pa@C_{60} is located at the small C2p subband consisting of two MOs corresponding to Γ_3 and Γ_4 irreducible representations of C_s double point group, in this cluster one orbital is occupied and one is vacant. The energy splitting between this C2p band (the admixtures of Pa5f AOs are near 10%) and the next unoccupied levels, corresponding to the states with main contribution from $5f_{5/2}$ AOs ($\sim$ 80%), is nearly 0.8 eV (Fig. 4). Although the Th5f, 6d and Pa5f, 6d molecular levels are vacant, the covalent mixing between $5f_{5/2}$, $5f_{7/2}$, $6d_{3/2}$, $6d_{5/2}$ and C2p orbitals in the occupied valence band leads to noticeable Mulliken population of 5f and 6d AOs, which were obtained as $5f_{5/2}^{0.43}$, $5f_{7/2}^{0.43}$, $6d_{3/2}^{0.54}$, $6d_{5/2}^{0.64}$ (Th@C_{60}) and $5f_{5/2}^{1.24}$, $5f_{7/2}^{0.92}$, $6d_{3/2}^{0.52}$, $6d_{5/2}^{0.59}$ (Pa@C_{60}).

In the next molecule of this row, U@C_{60}, the HOMO is still of C2p character, but the admixtures of U5f AOs increase up to 20%, while the LUMO in this cluster is of $5f_{5/2}$ character (82%). The energy gap between occupied and vacant levels is near 0.4 eV. Though the molecular orbitals containing main contributions from 5f AOs are still vacant in U@C_{60} cluster, the hybridization of $5f_{5/2}$, $5f_{7/2}$ and C2p AOs in the occupied molecular orbitals are responsible for the essential Mulliken populations of U5f AOs ($5f_{5/2}^{1.98}$ and $5f_{7/2}^{1.25}$), which are greater than those in Pa@C_{60}. In contrast, the populations of U6d orbitals ($6d_{3/2}^{0.51}6d_{5/2}^{0.57}$) are nearly the same as in protactinium complex. In the neptunium cluster, both HOMO and LUMO contain main contributions from Np$5f_{5/2}$ AOs (80%), i.e. the Fermi level is located in the $5f_{5/2}$ band. In addition, the admixtures of Np5f states in the occupied MOs of C2p character considerably increase (up to 35–40%). The filling of $5f_{5/2}$ states and increasing hybridization of $5f_{5/2}$, $5f_{7/2}$ and C2p AOs in the valence band are responsible for the essential Mulliken population of Np5f AOs: $5f_{5/2}^{2.76}5f_{7/2}^{1.55}$, on the other hand, the populations of Np6d orbitals decrease ($6d_{3/2}^{0.48}6d_{5/2}^{0.54}$) as compared to the uranium cluster.

The ground structures of the next three molecules of this row Pu@C_{60}, Am@C_{60} and Cm@C_{60} correspond to C_{2v} –type. In Figure 5, we show the partial DOS obtained in RDV calculations of Pu@C_{60} and Cm@C_{60} clusters. In the cases of C2s and C2p DOS we show only the contributions from two C1 and four C2 atoms, which are the nearest neighbors of metal ion. As can be seen from Fig. 5, the peaks corresponding to An$6p_{1/2}$ bands are shifted to lower energies by $\sim$ 11 eV (Pu) and $\sim$ 12 eV (Cm) from the highest intensity peak of An$6p_{3/2}$ DOS. In both complexes, the An$5f_{5/2}$ bands are completely occupied, however, between $5f_{5/2}$ and $5f_{7/2}$ states the small band of C2p character is located. This C2p band contains six MOs, two of which are occupied in Pu@C_{60} and three and four orbitals are occupied in Am@C_{60} and Cm@C_{60} clusters respectively. As a result, the An$5f_{7/2}$ MOs are vacant in all these systems, however, the admixtures of An$5f_{7/2}$ AOs in the highest occupied molecular states increase from 17% in Pu@C_{60} to 35% in Am@C_{60} and to 39% in Cm@C_{60}. Thus, the HOMO and LUMO in these three complexes are the mixture of C2p and An$5f_{5/2}$, $5f_{7/2}$ AOs. The strong hybridization of both $5f_{5/2}$ and $5f_{7/2}$ AOs with C2p orbitals in occupied MOs is responsible for the non-integer Mulliken population of 5f AOs, which increases from $5f_{5/2}^{3.71}5f_{7/2}^{2.14}$ in Pu@C_{60} to $5f_{5/2}^{4.35}5f_{7/2}^{2.55}$ in Am@C_{60} and to $5f_{5/2}^{4.95}5f_{7/2}^{3.02}$ in Cm@C_{60}. As mentioned above, the populations of An6d orbitals decreases for heavier actinides, the same trend was obtained for Pu@C_{60} ($6d_{3/2}^{0.35}6d_{5/2}^{0.33}$), Am@$C_{60}$ ($6d_{3/2}^{0.32}6d_{5/2}^{0.29}$) and Cm@$C_{60}$ ($6d_{3/2}^{0.25}6d_{5/2}^{0.21}$) complexes.

The occupied molecular orbitals of $5f_{7/2}$ character (51%, 57% and 73%) are firstly achieved in Bk@C_{60} (Fig. 6), as a result, the Mulliken populations of Bk5f states are $5f_{5/2}^{5.43}5f_{7/2}^{3.62}$, i.e. the total number of 5f electrons in Bk@C_{60} ($\sim$9.05) is greater than that in Cm@C_{60} ($\sim$7.97) by 1.08. The LUMO in Bk@C_{60} is also a mixture of Bk$5f_{7/2}$ (75%)
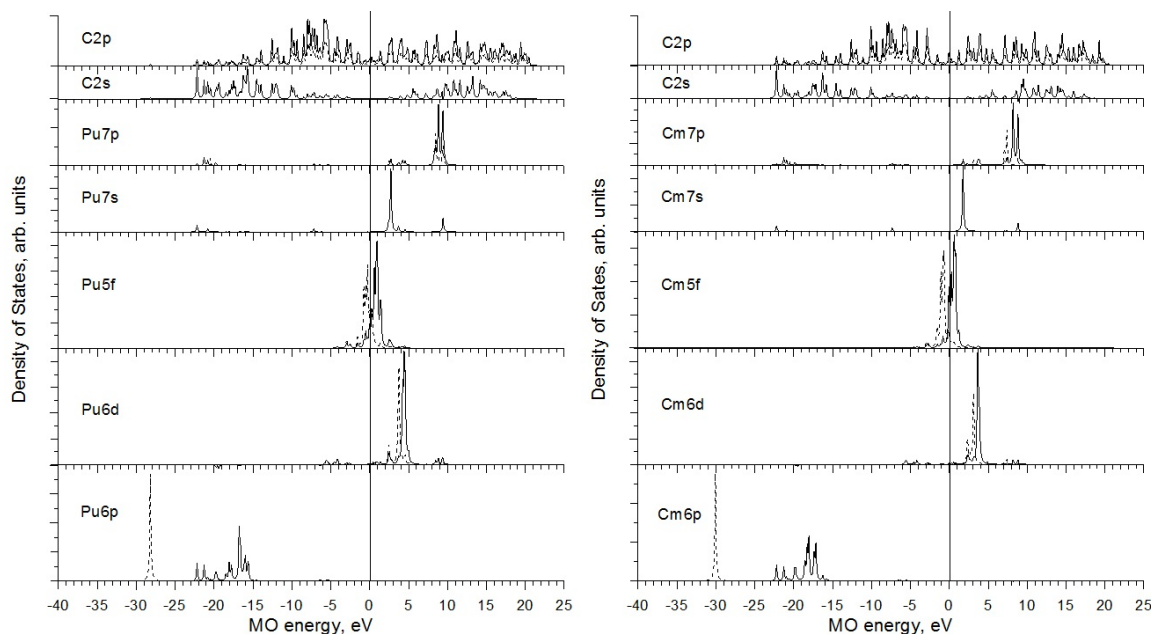
FIG. 5. Partial densities of states for the ground isomers of Pu@C$_{60}$ (left) and Cm@C$_{60}$ (right) clusters

and C2p AOs. On the other hand, the hybridization of Bk6d and C2p orbitals in the occupied C2p band is less than that in Cm@C$_{60}$, and a noticeable decrease of the Mulliken populations of Bk6d AOs was obtained ($6d_{3/2}^{0.18}6d_{5/2}^{0.12}$). Further filling of 5f shell and considerable depopulation of 6d shell were obtained for Cf@C$_{60}$ ($5f_{5/2}^{5.71}5f_{7/2}^{4.40}6d_{3/2}^{0.11}6d_{5/2}^{0.04}$) and Es@C$_{60}$ ($5f_{5/2}^{5.86}5f_{7/2}^{5.28}6d_{3/2}^{0.10}6d_{5/2}^{0.02}$). The complete occupation of both $5f_{5/2}$ and $5f_{7/2}$ molecular orbital types was achieved in the Fm@C$_{60}$ complex. The partial DOS obtained in RDV calculations of Fm@C$_{60}$ are shown in Fig. 6. The LUMO in Fm@C$_{60}$ are of almost purely C2p character (95%), the contributions from Fm5f AOs are nearly 3%. However, as a result of covalent mixing between the Fm atomic orbitals and the C$_{60}$ cage orbitals the Mulliken populations of 5f AOs are $5f_{5/2}^{5.93}5f_{7/2}^{6.20}$, i.e. the total number of 5f electrons in the Fm@C$_{60}$ cluster (12.1) is close to that of the isolated Fm atom. The energy gap between the occupied and vacant levels in Fm@C$_{60}$ is near 0.9 eV, which is the greatest value obtained in our calculations for endohedral fullerenes An@C$_{60}$. In the "last" investigated Md@C$_{60}$ complex, one more molecular orbital of C2p subband is occupied, thus both HOMO and LUMO are of almost purely C2p character and lie above the completely occupied Md5f$_{7/2}$ band by 0.4 eV. As expected, the admixtures of C2p AOs in the molecular orbitals of Md5f$_{7/2}$ type decrease and the Mulliken populations of Md5f shell are $5f_{5/2}^{5.98}5f_{7/2}^{7.16}$. As in the case of the fermium cluster, the total number of 5f electrons in the Md@C$_{60}$ molecule (13.1) is close to that of isolated Md atom.

To compare the effects of spin-orbit coupling for the valence orbitals of the systems at the beginning and at the end of An@C$_{60}$ series, one can use the splitting of the main peaks corresponding to $5f_{5/2}$ and $5f_{7/2}$ states. According to RDV calculations, the $5f_{5/2}$ – $5f_{7/2}$ peaks separation for Th@C$_{60}$, Pa@C$_{60}$, U@C$_{60}$ and Np@C$_{60}$ is close to 0.9 – 1.1 eV. For the Pu and Am complexes we obtained ∼1.2 eV, for Cm and Bk these values are close to 1.3 – 1.5 eV. In Cf@C$_{60}$ and Es@C$_{60}$ this spin-orbit splitting can be evaluated approximately as 1.6 – 1.7 eV. The noticeable increase of this value was obtained for the end of the row, i.e.
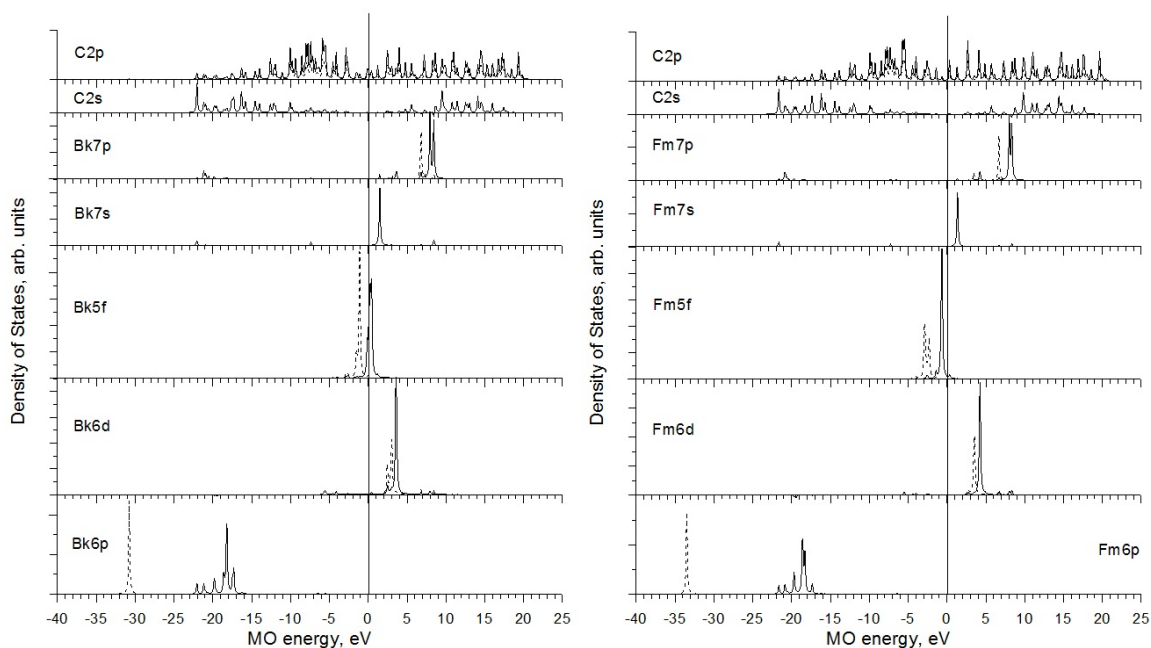
FIG. 6. Partial densities of states for the ground isomers of Bk@C_{60} (left) and Fm@C_{60} (right) clusters

for Fm@C_{60} and Md@C_{60} the splitting between $5f_{5/2}$ and $5f_{7/2}$ peaks is near 2.2 and 2.3 eV respectively (Fig. 6).

The molecular orbital structure of the most stable exohedral complex PaC$_{60}$ noticeably differs from that of the corresponding endohedral system. In Figure 7, we show the partial DOS obtained in RDV calculation of PaC$_{60}$ cluster. In the cases of C2s and C2p DOS we show only the contributions from two C1 atoms, which are the nearest neighbors of metal ion. As can be seen from Fig. 7, the hybridized C2s – Pa6p$_{3/2}$ subband in the energy region from -23 to -20 eV is absent in PaC$_{60}$, resulting in a more narrow distribution of 6p$_{3/2}$ DOS. The positions of Pa6d, 5f and 7s levels become closer to the Fermi level (Fig. 7). These shifts of the 6d, 5f and 7s states lead to noticeable increases in their contributions to molecular orbitals in this energy region, particularly the admixtures of Pa5f and 6d AOs in HOMO and LUMO achieve 19% and 10% respectively. Although the Pa5f and 6d orbitals are also vacant in the PaC$_{60}$ cluster, the hybridization of these states with occupied C2p orbitals leads to some Mulliken population of these AOs. According to our calculations, the occupations of these orbitals can be defined as $5f_{5/2}^{1.37}5f_{7/2}^{0.74}6d_{3/2}^{0.65}6d_{5/2}^{0.58}$. As seen, the populations of 5f AOs in PaC$_{60}$ are slightly less than those in Pa@C_{60}, while the populations of 6d AOs in PaC$_{60}$ are greater than those in Pa@C_{60} by 0.13. Surprisingly, in the case of a "networked" complex C$_{59}$Pa, we did not obtain the principal transformation of electronic structure (Fig. 7). The C2s – Pa6p$_{3/2}$ subband in the energy region from -23 to -20 eV is also absent in the C$_{59}$Pa cluster. The Pa6d, 5f and 7s DOS also shift to lower energies, however, their contributions in the valence band in the energy region from 0 to -4 eV become more important than those in endohedral and exohedral clusters. We can also note, that "networked" position of metal atom in the fullerene cage leads to some broadening of Pa6d, 7s and 7p bands in the energy region from 1 to 11 eV (Fig. 7).

The considerable hybridization between An5f and C2p AOs was obtained in all investigated fullerenes. However, the coefficients corresponding to An5f contribution in the molecular orbitals are not directly connected with the degree of 5f states delocalization. The
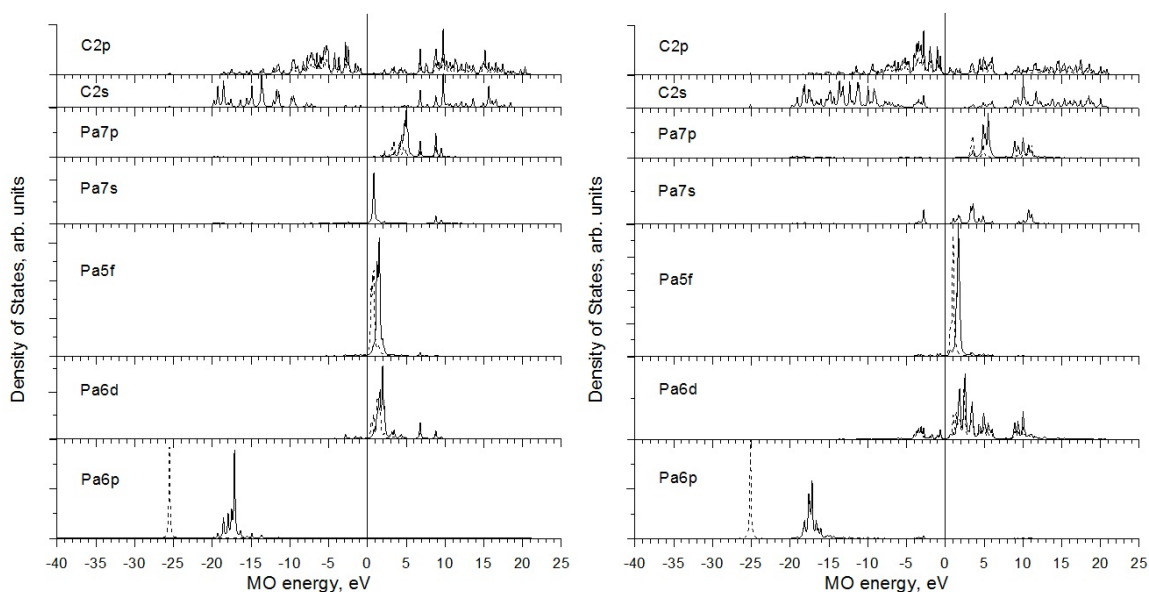
FIG. 7. Partial densities of states for the PaC_{60} (left) and $C_{59}Pa$ (right) clusters

latter effect could be evaluated qualitatively by an analysis of the shapes of corresponding molecular orbitals or more quantitatively by the values of overlap populations of various pairs of the metal and carbon AOs (n_{ij}). The values of n_{ij} can also give the bond orders of these states [17]. The values of overlap populations for C2p and 5f, 6d, 7s AOs of actinides obtained in our RDV calculations of endohedral clusters are listed in Table 2. As expected, the role of An7p-C2p interaction (not shown in Table 2) is anti-bonding in all investigated complexes.

TABLE 2. Overlap populations of An5f, 6d, 7s and C2p orbitals (10^{-3}e, per one pair of interacting atoms) in An@C_{60} complexes

Orbitals		Th	Pa	U	Np	Pu	Am	Cm	Bk	Cf	Es	Fm	Md
An5f -	$C_1$2p	36	41	37	32	22	18	12	8	3	2	1	0
	$C_2$2p	35	42	39	34	18	15	11	8	4	2	1	0
	$C_3$2p	35	39	36	31	-	-	-	7	3	1	1	0
An6d -	$C_1$2p	98	84	83	84	64	62	60	50	40	38	35	29
	$C_2$2p	97	83	85	84	50	49	49	46	41	37	35	27
	$C_3$2p	96	83	84	84	-	-	-	47	40	37	34	28
An7s -	$C_1$2p	15	16	16	16	9	9	10	12	9	9	10	3
	$C_2$2p	15	16	16	16	18	19	18	13	7	9	8	2
	$C_3$2p	14	16	16	16	-	-	-	13	8	7	9	2

Examination of Table 2 reveals that An6d orbitals play the main role in the chemical bonding of a metal atom and C_{60} cage in all of An@C_{60} clusters. This result is quite expected, because in our earlier relativistic calculations of actinide oxides, fluorides [18,19] and An@C_{40} clusters [3], the main contributions to bonding was also provided by An6d AOs and the next An5f contributions to bonding were considerably less. However, the earlier calculations of small endohedral fullerenes An@C_{28} [2] showed that An6d and 5f orbitals play comparable roles in the chemical bonding of a metal atom and C_{28} cage in the first

half of the An@C_{28} row. This difference in the bonding behavior of An5f states in An@C_{40}, An@C_{60} and An@C_{28} can be explained by the well known fact that An5f AOs participation in bonding is sensitive to the distances between actinide atom and its neighbors [19]. As mentioned above, the shortest An–C bond lengths in An@C_{40} and non-symmetrical An@C_{60} clusters are greater than the longest An–C bond lengths in An@C_{28} systems. As shown in Table 2, the overlap populations of An5f–C2p states increase when going from Th@C_{60} to Pa@C_{60} clusters and then monotonously decrease to zero at the end of this row. However, noteworthy is the considerable decrease of An5f contributions to bonding on going from Np@C_{60} to Pu@C_{60}. On the other hand, the slightly non-monotonous bonding behavior at the beginning of An@C_{60} row is detected for An6d orbitals. As can be seen from Table 2, a small increase of overlap populations for An6d–C2p states takes place for the U@C_{60} and Np@C_{60} molecules in comparison to the Pa@C_{60} cluster.

     Comparison of the stability of endohedral complexes (Table 1) and corresponding bond orders (Table 2) shows that there is good correlation between DMol and RDV results. The increase of the dissociation energy (An@$C_{60} \rightarrow$ An + C_{60}) when going from Th@C_{60} to Pa@C_{60} is in agreement with the increase of contribution to bonding from Pa5f states, note that this contribution is the greatest in An@C_{60} row (Table 2). Further decrease of stability from Pa to Am correlates with a decrease of the overlap populations for An5f–C2p as well as for An6d–C2p AOs. The small increase of $|E_b|$ for Cm@C_{60} and Bk@C_{60} clusters (Table 1) can be explained by the role of spin-polarization, which is included in the scalar-relativistic DMol calculations, but is not treated in the standard Dirac theory. Note, that similar results were also obtained for An@C_{40} complexes [3].

     The values of overlap populations for C2p and 5f, 6d, 7s AOs of protactinium obtained in our RDV calculations for the exohedral and "networked" complexes are listed in Table 3. The corresponding parameters for endohedral cluster are also shown in Table 3 for comparison. Note, that n_{ij} values presented in Tables 2 and 3 correspond to one pair of interacting atoms, hence, the sum of these values for the six nearest neighbors in endohedral cluster will be considerably greater than total overlap populations in exohedral system. However, as can be seen from Table 3, the interactions between actinide and a specific carbon atom in the C_{59}Pa and PaC_{60} are stronger than that in Pa@C_{60} complex. Examination of Table 3 reveals that Pa6d orbitals also play the main role in chemical bonding of metal atom and carbon cage in these clusters. The variation of n_{ij} for the Pa5f–C2p and Pa6d–C2p bonds also correlates with Pa–C bond lengths (Table 1). As shown in Table 3, the interaction between protactinium atom and each of three nearest neighbors in "networked" complex is considerably stronger than that in more stable endohedral cluster. However, as mentioned above, the actinide – carbon substitution in C_{60} cage is energetically disfavored process and the formation of C_{59}Pa complex does not provide a better way for the extraction of the actinides from some species.

     The effective charges on actinide atoms (Q_{An}) obtained in our scalar relativistic (DMol) and fully relativistic calculations (RDV) are listed in Table 1. As shown, the effective charges obtained in DMol calculations using Hirshfeld scheme correlate with neither the variation of binding energy nor with the variation of An–C bond lengths. It is quite evident that the increase in charge transfer for the Pu@C_{60} and Am@C_{60} in comparison with Np@C_{60} as well as for the second half of the series (from Bk to Md) in comparison with Cm@C_{60} and the weaker interaction between cage and actinide atom are contradictory. On the other hand, the integral charges obtained in RDV calculations (Table 1) agree with the variation in the binding energy. Although the Q_{An} obtained in relativistic calculations are considerably greater than the DMol values, the effective charges on actinide atoms are less

TABLE 3. Overlap populations of An5f, 6d, 7s and C2p orbitals (10^{-3}e, per one pair of interacting atoms) in exohedral PaC_{60}, "networked" $C_{59}Pa$ and endohedral $Pa@C_{60}$ complexes

Orbitals		PaC_{60} (C_{2v})	$C_{59}Pa$ (C_s)	$Pa@C_{60}$ (C_s)
Pa5f -	$C_1$2p	46	67	41
	$C_2$2p	-	51	42
	$C_3$2p	-	-	39
Pa6d -	$C_1$2p	90	148	84
	$C_2$2p	-	112	83
	$C_3$2p	-	-	83
Pa7s -	$C_1$2p	24	36	16
	$C_2$2p	-	34	16
	$C_3$2p	-	-	16

than their formal valencies in solid compounds. The comparison of Tables 1 and 2 shows that the variation of the integral charges on going from $Th@C_{60}$ to $Md@C_{60}$ is mainly due to the decrease of An6d–C2p covalent mixing and overlap of these orbitals.

Although the chemical bonding between actinide atom and the carbon cage is weak for the clusters at the end of $An@C_{60}$ row, both the DMol and RDV calculations exhibit essential charge transfers of more than 0.6 electron from the actinide orbitals to the cage. Similar results were obtained in our calculations of $An@C_{40}$ row [3]. From our point of view, there is no contradiction between binding energy and charge transfer because a change in binding energy on going from superposition of isolated C_{60} (or C_{40}) cage and actinide atom to endohedral complex is due to contributions from: (1) interaction between actinide and the carbon atoms and (2) deformation of the initial fullerene structure. The latter contribution is certainly unfavorable and even in the case of $Md@C_{60}$ complex the interaction between metal and carbon atoms has the bonding character. On the other hand, the strong C–C bonds in the C_{60} (or C_{40} and C_{28}) cage are not accompanied by noticeable charge transfer, whereas in the $C_{59}Pa$ complex the considerable charge transfer (more than 2 electrons) was obtained for the weaker Pa–C bonds.

According to our calculations of endohedral complexes, the additional charge on the cage orbitals is distributed over all carbon atoms, i.e. the deformation of electron density takes place even for the carbon atoms, which are the most distant from actinide site. However, as expected, variation of the charge density on the nearest actinide neighbors is slightly greater than that for other atoms of the cage. Nevertheless, the effective charges on C1, C2 and C3 atoms are within -0.1 in endohedral fullerenes of the first half of the row and within -0.05 for the complexes of heavy actinides. In contrast, the main part of charge transfer from the metal atom in the exohedral and especially in the "networked" clusters is localized on the nearest carbon neighbors. For instance, in the $C_{59}Pa$ complex, the integral charges on one C1 and two C2 atoms are -0.76 and -0.67 respectively, i.e. the total electron density, which is accepted by these carbon atoms is close to 2.1.

4. Conclusions

Our investigations of the new class of organometallic nanoparticles An@C_{60} confirm earlier results [1-3] that endohedral fullerenes can be very stable. Moreover, the stable character of such species for the light actinides obtained for the An@C_{28} and for the major part of An@C_{40} clusters (from Th to Fm) is also predicted for the neutral endohedral fullerenes An@C_{60} from Th@C_{60} to Md@C_{60}. The dissociation energy for the most stable complex Pa@C_{60} (Pa@$C_{60} \rightarrow$ Pa + C_{60}) was found to be 6.6 eV, which is noticeably greater than that for the exohedral position of Pa atom on the outer surface of C_{60} cage. Comparison of the electronic structure of endohedral complexes based on C_s and I_h isomers showed that the former type is more favorable for the encapsulation of an actinide atom.

Analysis of the molecular orbital structure showed that strong hybridization takes place between C2p and An5f states for all An@C_{60} complexes. However, the calculated values of overlap populations of C2p–An5f AOs showed that the An5f contribution to bonding was more than two times less than that of the main An6d–C2p interaction, even in the neutral clusters at the beginning of An@C_{60} row. The analysis of chemical bonding of endohedral, exohedral and "networked" fullerenes showed that the strongest interaction between actinide atom and specific carbon atom in the C_{60} cage takes place for "networked" complex. However, the stability of the latter cluster is less than that of the corresponding endohedral systems, because: (1) in C_{59}Pa molecule the three Pa–C bonds substitute for the three stronger C–C bonds; (2) in An@C_{60} complexes the An–C interactions are additional to the C–C bonds in the cage. Two schemes for atomic effective charge calculations give quite different results for An@C_{60}, however, more realistic values were obtained using the spatial numerical integration procedure incorporated into the RDV method [16].

In this paper, we discussed the stability of endohedral fullerenes An@C_{60} with respect to the An + C_{60} fragmentation only. However, for the understanding of stability of these systems, it is important to consider the other competitive processes which can happen when An@C_{60} systems will ionize. It is interesting to calculate the ionization energy and the dissociation energy of An@C_{60}^{n+} systems, this work is in progress now and will be published in the separate paper.

Acknowledgments

References

[1] Dognon J.-P., Clavaguera C., Pyykko P. A predicted organometallic series following a 32-electron principle: An@C_{28} (An = Th, Pa$^+$, U^{2+}, Pu^{4+}). *J. Amer. Chem. Soc.*, **131**, P. 238–243 (2009).

[2] Ryzhkov M.V, Ivanovskii A.L., Delley B. Electronic structure of endohedral fullerenes An@C_{28} (An = Th – Md). *Comp. Theor. Chem.*, **985**, P. 46–52 (2012).

[3] Ryzhkov M.V., Delley B. Electronic structure of predicted endohedral fullerenes An@C_{40} (An = Th – Md). *Comp. Theor. Chem.*, **1013**, P. 70–77 (2013).

[4] Kroto H.W., Heath J.R., O'Brien S.C., Curl R.F., Smalley R.E. C-60 buckminsterfullerene. *Nature*, **318**, P. 162–163 (1985).

[5] Diener M., Smith C.A., Veirs D.K. Anaerobic preparation and solvent-free separation of uranium endohedral metallofullerenes. *Chem. Mat.*, **9**, P. 1773–1777 (1997).

[6] Chang A.H.H., Ermler W.C., Pitzer R.M. The ground and excited states of C60M and C60M+ (M = O, F, K, Ca, Mn, Cs, Ba, La, Eu, U). *J. Chem. Phys.*, **94**, P. 5004–5010 (1991).

[7] Delley B. An all-electron numerical method for solving the local density functional for polyatomic molecules. *J. Chem. Phys.*, **92**, P. 508–517 (1990).

[8] Koelling D.D., Harmon B.N. A technique for relativistic spin-polarized calculations. *J. Phys. C: Solid State Phys.*, **10**, P. 3107–3114 (1977).

[9] Perdew J.P., Burke K., Ernzerhof M. General gradient approximation made simple. *Phys. Rev. Lett.*, **77**, P. 3865–3868 (1996).

[10] Becke A.D. A multicenter numerical-integration scheme for polyatomic molecules. *J. Chem. Phys.*, **88**, P. 2547–2553 (1988).

[11] Lee C., Yang W., Parr R.G. Development of the Colle-Salvetti correlation-energy formula into a functional of the electron-density. *Phys. Rev.B.*, **37**, P. 785–789 (1988).

[12] Rosen A., Ellis D.E. Relativistic molecular calculations in the Dirac-Slater model. *J. Chem. Phys.*, **62**, P. 3039–3049 (1975).

[13] Adachi H. Relativistic molecular orbital theory in the Dirac-Slater model. *Technol. Reports Osaka Univ.*, **27**, P. 569–576 (1977).

[14] Pyykko P., Toivonen H. Tables of representation and rotation matrices for the relativistic irreducible representations of 38 points groups. *Acta Acad. Aboensis, Ser.B.*, **43**, P. 1-50 (1983).

[15] Varshalovich D.A., Moskalev A.N., Khersonskii V.K. *Quantum Theory of Angular Momentum.* World Scientific, Singapore, 439 p. (1988).

[16] Ryzhkov M.V. New method for calculating effective charges on atoms in molecules, clusters and solids. *J. Struct. Chem.*, **39**, P. 933–937 (1998).

[17] Mulliken R.S. Chemical bonding. *Annu. Rev. Phys. Chem.*, **29**, P. 1-30 (1978).

[18] Ryzhkov M.V., Kupryazhkin A.Ya. First-principles study of electronic structure and insulating properties of uranium and plutonium dioxides. *J. Nuclear Mater.*, **384**, P. 226–230 (2009).

[19] Ryzhkov M.V., Teterin A.Yu., Teterin Yu.A. Fully relativistic calculations of ThF$_4$. *Int. J. Quant. Chem.*, **110**, P. 2697–2704 (2010).